Stability of thermoviscous Hele-Shaw flow

By S. J. S. MORRIS

Department of Mechanical Engineering, University of California, Berkeley, CA 94720, USA

Viscous fingering can occur as a three-dimensional disturbance to plane flow of a hot thermoviscous liquid in a Hele-Shaw cell with cold isothermal walls. This work assumes the principle of exchange of stabilities, and uses a temporal stability analysis to find the critical viscosity ratio and finger spacing as functions of channel length, L_c. Viscous heating is taken as negligible, so the liquid cools with distance (x) downstream. Because the base flow is spatially developing, the disturbance equations are not fully separable. They admit, however, an exact solution for a liquid whose viscosity and specific heats are arbitrary functions of temperature. This solution describes the neutral disturbances in terms of the base flow and an amplitude, $A(x)$. The stability of a given (computed) base flow is determined by solving an eigenvalue problem for $A(x)$, and the critical finger spacing. The theory is illustrated by using it to map the instability for variable-viscosity flow with *constant* specific heat. Two fingering modes are predicted, one being a turning-point instability. The preferred mode depends on L_c. Finger spacing is comparable with the thermal entry length in a long channel, and is even larger in short channels. When applied to magmatic systems, the results suggest that fingering will occur on geological scales only if the system is about freeze.

1. Introduction

Melt flow in a channel is prone to fingering in the plane of the wall, owing to coupling between heat advection and temperature-dependent flow resistance. Fingering can develop as melt fills the channel, or as an instability of flow established in a full channel. In the first case, fingers are visible on the filling front, as in Whitehead & Helfrich (1991, plate 1). Such fingers are preserved in solidified sheet intrusions of magma (Pollard, Muller & Dockstader 1975; figure 8). This type of fingering may also occur during polymer moulding (Pearson 1985; pp. 227,591). Fingering on an established base flow is observed during basaltic fissure eruptions. Over time, eruption from an initially linear crack is confined to few isolated vents (Richter *et al.* 1970; Delaney & Pollard 1982). Fingering in melts is explained physically by Pearson, Shah & Vieira (1973). A liquid column parallel to the primary flow, and slightly hotter than neighbouring columns, flows faster than they, and cools more slowly. A spanwise thermal perturbation thus induces fingering unless suppressed by conduction to the wall. The instability might also occur on sheet-like upwellings in Earth's solid mantle, where creep is temperature-dependent (Whitehead & Helfrich 1991, p. 4155).

Melt fingering is similar to the Saffman–Taylor instability as both are driven by a streamwise gradient in viscosity or effective permeability (see (4), below). The two instabilities *differ* in the boundary conditions. When the Saffman–Taylor instability occurs on the displacement front separating two miscible fluids, such as water and

glycerine or CO_2 and oil, the walls are in effect insulated and diffusion occurs only parallel to the walls. The base flow is unsteady, but one-dimensional. But in melt flow, diffusion across the thin gap is dominant, and the base flow is a thermal entry flow in which the two dynamically significant temperature gradients are mutually perpendicular. This has both physical and technical implications. The critical viscosity ratio is greater than one for melt fingering, but is one for the Saffman–Taylor instability of a plane base flow of two miscible fluids (Tan & Homsy 1986, equation 44). Also, analysis of the melt flow appears at first to be complicated. The base flow must be computed numerically, the disturbance equations are complicated, and not separable in general. This complexity hides the physics of the instability.

Two ways have been tried to circumvent this difficulty. Pearson *et al.* (1973) study the instability with a simplified model resembling a Galerkin analysis of the viscous flow. Derivatives representing diffusion of heat and momentum across the channel gap are replaced by multiples of the mean temperature and velocity. The model admits a solution representing plane flow, and this loses stability to fingers above a critical viscosity ratio. The study is suggestive but, as the authors note, not definitive since the temperature profile varies downstream as the flow adjusts to the change in boundary conditions. A second approach has been tried by Morris (1988): see Appendix C, below. The Hele-Shaw equations admit a parallel-flow solution if the wall temperature decreases linearly downstream, and the viscosity $\mu = \mu_0 e^{-\gamma T}$. The disturbance equations are then separable, and fingering occurs as a turning-point instability. Further analysis is needed to see if this result is typical of more realistic flows.

The present work is a precise treatment of the temporal stability of the thermal entry flow modelled qualitatively by Pearson *et al.* It provides a solution suitable for testing approximate analyses of more realistic and complex models of geological flows. Here is the approach. Section 2 derives the stream function–vorticity formulation for three-dimensional thermoviscous channel flow. Section 3 shows that to each steady plane solution of these equations, there corresponds a *family* of steady three-dimensional flows. The structure of these flows in the thin dimension of the channel is determined by the parent plane flow. The variation parallel to the walls is governed by a pair of coupled *two-dimensional* partial differential equations. The exact solution thus expresses the three-dimensional flow in terms of a pair of two-dimensional flows: without approximation, it has the desirable properties of a Galerkin analysis. It is used later, in §9, to interpret the results of the linear stability analysis of the plane flow. Section 4 states the equations governing arbitrary infinitesimal disturbances, and §5 gives an explicit solution to the disturbance equations. This solution shows, without approximation, that a set of disturbances exists for which the stability problem reduces to an eigenvalue problem for an ordinary differential equation. The coefficients of this equation depend on the plane base flow, and are computed by finite-difference solution of the thermal entry flow, as described in §6. The explicit solution of the disturbance equations removes the technical complications described in the previous paragraph, and shows the stability of the base flow is determined by the pressure gradient rather than by details of the velocity and temperature profiles. Although the solution describes a particular class of disturbances, physical reasoning suggests that this class contains the most unstable disturbances. There is a second reason for believing the disturbances physically relevant. The *form* of the eigenvalue problem solved in the Galerkin analysis of Pearson *et al.* is identical with that solved here. (The coefficients differ because Pearson's model does not closely represent the pressure gradient in the viscous flow.) The present analysis therefore coincides with
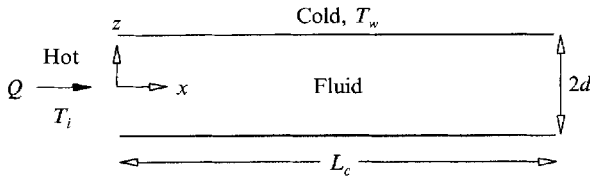
FIGURE 1. Definition sketch. Fingering occurs in the third (y) dimension.

the Galerkin analysis, except in those details where the Galerkin analysis is plainly questionable. Sections 7 and 8 discuss the numerical solution of the eigenvalue problem, and its predictions. Lastly in §9, the linear stability analysis is interpreted in the light of the exact three-dimensional solution given in §3.

The principle of exchange of stabilities is assumed here, i.e. neutral disturbances are assumed steady. This is justified because Pearson *et al.* found only real growth rates in analysing their model. (Their Galerkin analysis does not accurately represent all details of the flow, but should describe such a qualitative property.) Because the growth rates are real even at supercritical viscosity ratios, the unstable disturbance is not convected downstream but grows at each point in the flow. The instability is thus *absolute* rather than *convected*, in the sense used in studies of shear layer stability (e.g. Landau & Lifshitz 1987, §28). Absolute instability is possible in this flow because the equation for the pressure is elliptic, so the disturbance is felt throughout the flow, and because boundary conditions tie the temperature field to a given entry region.

2. Statement of the problem

Figure 1 shows the geometry. The channel has length L_c and thickness $2d$. The base flow occupies the $(x, 0, z)$-plane, with the primary flow parallel to Ox. Fingering occurs in the third (y) dimension. The wall and inlet temperatures (T_w, T_i) are both constants. The velocity (V) vanishes on both walls. The pressure (p) is fixed at $x = 0$ and $x = L_c$.

Material properties other than viscosity, $\mu(T)$, and specific heat, $c(T)$, are taken as constant. This is a good approximation for viscous melts like magma, see Murase & McBirney (1973). The two explicit solutions given here, namely (6) and (11), hold for arbitrary $\mu(T)$ and $c(T)$. Freezing of materials whose liquid and solid states have the same density can thus be included by taking $c(T)$ as a suitable generalized function of T. In this work, however, these explicit solutions are explored in detail only for *constant* specific heat.

Let Q be volume flow rate per unit width in the base flow; and κ, thermal diffusivity at the inlet temperature. Let $Pe = Q/\kappa$ and $L_e = dPe$. (L_e is the thermal entry length, i.e. the distance travelled downstream by a particle moving with velocity Q/d in the time needed for heat to diffuse across the channel gap.) Define dimensionless (without asterisks) variables by

$$(x, y)_* = L_e(x, y), \quad z_* = zd, \quad (u, v)_* = \frac{Q}{d}(u, v), \quad w_* = \frac{\kappa}{d}w,$$

$$p_* = \mu_w \frac{Q}{d^3} L_e p, \quad T_* - T_w = T\ (T_i - T_w).$$

Also $c_*(T) = c_i c(T)$ and $\mu_*(T) = \mu_w \mu(T)$, where subscripts i and w denote conditions

at the inlet and wall temperatures. The dimensionless channel length is $X = L_c/L_e = \kappa L_c/Qd$, by definition of L_e.

Throughout this work, a prime denotes differentiation of a function of a single variable.

The thermal entry length is assumed large compared with the gap width. Fluid acceleration and viscous heating are assumed negligible. The first assumption holds because $Pe \gg 1$ in the flows of interest, and implies that the slope (α) of the streamlines is small: specifically, $\alpha \sim d/L_e \sim Pe^{-1}$. Lubrication theory is therefore appropriate: streamwise diffusion of heat and momentum is negligible, and p is uniform in z, as in (1) below. In lubrication flows, fluid acceleration is negligible if $\alpha Re \ll 1$, where $Re = \rho V d/\mu$. Here $\alpha \sim Pe^{-1}$, so that $\alpha Re \sim Pr^{-1}$. Fluid acceleration is thus negligible, since the Prandtl number $Pr \gg 1$ for melts. Lastly, viscous heating is taken as negligible because the Brinkman number $Br = \mu V^2/k\Delta T$ is small in many dyke flows. Delaney & Pollard (1982) estimate the following values as typical of magma flow in dykes: $V \sim 0.5$ m s^{-1}, dyke thickness $d \sim 2$ m, $\mu \sim 10^2$Pa s, thermal conductivity $k \sim 2$W m^{-1}K^{-1}, thermal diffusivity $\kappa \sim 10^{-6}$m^{2}s^{-1}, and $\Delta T \sim 10^3$K. For such a flow, $Br \sim 10^{-2}$, $Pr \sim 10^5$, and $Pe \sim 10^6$.

The governing Hele-Shaw equations are obtained formally by writing the equations for isochoric creeping flow in dimensionless variables, and taking the limit $Pe \to \infty$ with (x, y) fixed. They are

$$\nabla p = (\mu \mathbf{v}_z)_z, \quad p_z = 0, \tag{1a,b}$$

$$c\mathbf{V} \cdot \mathrm{grad}\, T = T_{zz}, \quad \mathrm{div}\, \mathbf{V} = 0. \tag{1c,d}$$

Here $c(T)$ is the specific heat, as noted above. Subscripts denote differentiation. grad and $\mathbf{V} = u\mathbf{i} + v\mathbf{j} + w\mathbf{k}$ are the three-dimensional gradient operator and velocity; ∇ and $\mathbf{v}$ are the components of these quantities in the (x, O, y)-plane, i.e. $\mathbf{v} = \mathbf{V} - w\mathbf{k}$, and $\nabla = \mathrm{grad} - \mathbf{k}\partial/\partial z$.

(To avoid confusion, we note that a type of Hele-Shaw approximation is also used to study injection moulding of polymers. In that literature, the term wT_z representing convection of heat perpendicular to the walls is taken as zero if the walls are parallel (e.g. Dupret & Dheur 1992, p. 586). The present work *includes* the term wT_z: it is, of course, comparable in magnitude to the other convective terms in (1c).)

Equation (1d) is satisfied by introducing two stream functions, namely $\psi(x, y)$ and $\phi(x, y, z)$. Appendix A shows that the velocity in Hele-Shaw flow (1) can be written as

$$u = \psi_y \phi_z, \quad v = -\psi_x \phi_z, \quad w = \psi_x \phi_y - \psi_y \phi_x, \tag{2}$$

where $\phi(x, y, \pm 1) = \pm 1/2$. ψ is a stream function for the volume transport, because integration of (2) over z shows that $\int_{-1}^{1} u(x, y, z)\, \mathrm{d}z = \psi_y$ and $\int_{-1}^{1} v(x, y, z)\, \mathrm{d}z = -\psi_x$.

The equation for ϕ follows by elimination of p between (1a) and (1b). Thus $(\mu \mathbf{v}_z)_{zz} = 0$. Substitution for $\mathbf{v}$ from (2), followed by integration in z, gives

$$0 = zK^{-1} + \mu \phi_{zz}. \tag{3}$$

$K(x, y)$ is an arbitrary function of integration, determined by the second-order equation (3) and three boundary conditions, namely $\phi = 1/2$, $\phi_z = 0$ at $z = 1$, and $\phi = 0$ at $z = 0$. $K(x, y)$ depends *implicitly* on the temperature distribution in the channel: specifically, (3) and the boundary conditions can be solved for K, to show that without approximation $K = \int_{-1}^{1}(z^2/\mu)\, \mathrm{d}z$.

The equation for ψ follows by manipulating (1a), (1b) and (3) to get the (z-averaged) equation for the z-component of vorticity. First, these equations imply that

$-Kp_x = \psi_y$ and $Kp_y = \psi_x$. K is thus the effective permeability of the Hele-Shaw cell. Secondly, elimination of p shows that the equation for ψ is

$$\nabla \cdot \frac{1}{K}\nabla\psi = 0, \tag{4}$$

i.e. $\nabla^2\psi = \nabla\psi \cdot \nabla\ln K$. This is satisfied by plane flow, in which $\psi = y$ and K depends only on x. But the right-hand side is not zero if K varies across lines of constant ψ. A three-dimensional disturbance to the plane flow thus induces transverse vorticity $(-\nabla^2\psi)$. The induced motion tends to amplify the disturbance if K decreases downstream (compare Tan & Homsy 1988, equation 31).

The flow is determined by (1c), (3), (4), and the boundary conditions.

3. A family of steady solutions including plane flow

The governing equations admit the plane solution $\bar{\psi} = y$, $\phi = \Phi(x,z)$, $T = \bar{T}(x,z)$, $K = \bar{K}(x)$, so that $\bar{V} = U\boldsymbol{i} + W\boldsymbol{k}$ where $U = \Phi_z$ and $W = -\Phi_x$.

The plane flow satisfies

$$\bar{c}\bar{V} \cdot \operatorname{grad}\bar{T} = \bar{T}_{zz} \quad\text{and}\quad 0 = z\bar{G} + \bar{\mu}U_z, \quad\text{where}\quad \bar{G} \equiv \bar{K}^{-1}. \tag{5a,b}$$

$\bar{c} \equiv c(\bar{T})$ is the specific heat, as defined in §2. $\bar{G}$ is the pressure gradient in the plane flow, i.e. $\bar{G} = -\bar{p}'(x)$.

The flow is an even function of z, because the inlet flow is even. On $z = 1$, $U = 0 = T$, and $\Phi = 1/2$. On $z = 0$, $\Phi = 0 = \bar{T}_z$. At $x = 0$, $T = 1$.

Two properties of the plane flow are important for the linear stability analysis. First, each plane flow (5) generates a *family* of three-dimensional solutions of (1c), (3) and (4). Let $\xi(x,y)$ be an arbitrary function such that $\xi(0,y) = 0$. By substitution, (3) is satisfied if

$$T = \bar{T}(\xi,z), \quad \phi = \Phi(\xi,z) \quad\text{and}\quad K = 1/\bar{G}(\xi). \tag{6}$$

Equations (4) and (1c) are satisfied if

$$\nabla \cdot \bar{G}(\xi)\nabla\psi = 0 \quad\text{and}\quad \psi_y\xi_x - \psi_x\xi_y = 1. \tag{7a,b}$$

The variable specific heat and viscosity enter (7) *implicitly* through $\bar{G}$.

The three-dimensional solution (6) satisfies the same boundary conditions as the plane flow, because ξ vanishes at $x = 0$. The solution is determined by the plane flow (5), and the solution of the two-dimensional partial differential equations (7). As noted in §1, this solution therefore has the desirable properties of a Galerkin analysis, without approximation.

The steady solution of (7) is not unique in general. One solution is the plane flow $\psi = y$ and $\xi = x$. A second, non-planar solution exists above a critical viscosity ratio, as shown by the following linear stability analysis of the full problem (1). See also (17), below.

Equation (7) expresses precisely the physical mechanism described in the opening paragraph of §1. Let t be the time passed since a particle moving with velocity $\psi_y, -\psi_x$ crossed the line $x = 0$. Then the characteristic equations of (7b) are $\dot{\xi} = 1, \dot{x} = \psi_y, \dot{y} = -\psi_x$, where the dot denotes the time derivative. Integration of the first equation shows that $\xi = t$, because ξ vanishes at $x = 0$ by its definition above. ξ is thus the time passed since the particle crossed the line $x = 0$. Within a hot finger, $\bar{G}$ is relatively small, and the vorticity equation (7a) acts to focus the flow, as explained following (4). The time (t) needed for a particle in a hot finger to travel a given distance is

therefore relatively small, as is ξ. Equation (6) then shows that in a hot finger T tends to stay close to the inlet temperature. Pearson (1976) described the instability as resulting from a modification of the path length through the Hele-Shaw cell. The present exact solution gives a simple explicit formulation of that idea. Equation (7) is used to interpret the linear stability analysis.

A second property of the plane flow is used in §7 in discussing the turning-point instability. The velocity, temperature and pressure gradient in the plane flow are independent of channel length (X), because the governing equations (5) are parabolic. As in isoviscous Poiseuille flow, X enters only when $\bar{G}(x)$ is integrated over x to find the pressure drop–flow rate relation.

For this work, (5) was solved by modifying a standard finite-difference method for momentum boundary layers (e.g. Blottner 1975). Briefly, (5) is transformed to remove the singularity at $x = 0$ and $|z| = 1$. Three-point backward differences are used in x and centred differences in z. The scheme is implicit, second order in dz, but only first order in dx, in practice. At each x, the nonlinear difference equations were solved by Picard iteration. This proves essential for accurate solutions at large viscosity ratios. Appendix B gives details.

4. Equations for infinitesimal three–dimensional disturbances

Let $\delta\phi, \dots$ be three-dimensional disturbances to the plane flow (5). (These disturbances are arbitrary: the three-dimensional flow is not restricted to be of the form (6).) Then $\{\psi, \phi, T, K\} = \{y, \bar{\Phi}, \bar{T}, \bar{K}\} + \{\delta\psi, \delta\phi, \delta T, \delta K\}$. The equations for infinitesimal disturbances follow, as usual, by substitution in the governing equations, subtraction of the equations for the base flow, and then taking as zero all products of disturbance quantities. The neutral disturbances are taken as steady, i.e. exchange of stabilities is assumed. As noted in §1, this analysis determines the absolute stability of the base flow. Disturbances will therefore grow in time at any fixed point in the flow if the viscosity ratio exceeds the critical value found here.

The coefficients of the disturbance equations depend only on x and z since the base flow is independent of y. The equations can therefore be Fourier transformed in y. Thus, let $\{\delta\psi, \delta\phi, \delta T, \delta K\} = \{i\hat{\psi}(x), \hat{\phi}(x,z), \hat{T}(x,z), \hat{K}(x)\}e^{iay}$. A hatted variable is the Fourier transform in y of the corresponding disturbance.

Let the transform of the disturbance velocity be $\hat{V} = \hat{u}i + \hat{v}j + \hat{w}k$, where from (2)

$$\hat{u} = -a\hat{\psi}U + \hat{\phi}_z, \quad \hat{v} = -iU\hat{\psi}', \quad \hat{w} = -a\hat{\psi}W - \hat{\phi}_x. \qquad (8a,b,c)$$

(A prime denotes differentiation of a function with a single argument, as stated in §2.) Notice that all *three* components of the disturbance velocity are included in the analysis, as previously stated following (1).

Without approximation, infinitesimal disturbances satisfy

$$(\bar{G}\hat{\psi}')' - a^2\bar{G}\hat{\psi} = a\bar{G}^2\hat{K}, \quad \mu(\bar{T})\hat{\phi}_{zz} + \mu'(\bar{T})U_z\hat{T} = z\bar{G}^2\hat{K}, \qquad (9a,b)$$

$$\bar{c}\bar{V} \cdot \operatorname{grad}\hat{T} = \hat{T}_{zz} - \bar{c}\hat{V} \cdot \operatorname{grad}\bar{T} - \hat{T}\bar{V} \cdot \operatorname{grad}\bar{c}. \qquad (9c)$$

On $z = 1$, $0 = \hat{\phi} = \hat{\phi}_z = \hat{T}$.   On $z = 0$, $\hat{T}_z = 0 = \hat{\phi}$. $\qquad (10a)$

At $x = 0$, $\hat{T} = 0 = \hat{\psi}'$.   At $x = X$, $\hat{\psi}' = 0$. $\qquad (10b)$

The last term on the right-hand side of the disturbance energy equation (9c) is

the perturbation due to the variable heat capacity. Specifically, this perturbation is $(\delta c)\bar{V} \cdot \mathrm{grad}\,\bar{T} = \hat{T}c'(\bar{T})\bar{V} \cdot \mathrm{grad}\,\bar{T} = \hat{T}\bar{V} \cdot \mathrm{grad}\,\bar{c}$, as in (9c).

Equations (9) and (10) define the eigenvalue problem for the wavenumber a as a function of viscosity ratio. The coefficients of the eigenvalue problem are purely real, and the functions $\hat{\psi}$, $\hat{\phi}$, $\hat{T}$ and $\hat{K}$ are real valued (i enters the problem only through the expression (8b) for $\hat{v}$, and the eigenvalue problem is independent of $\hat{v}$).

The five conditions (10a) specify the solution at each x because (9) is fourth-order in z, and contains a function $\hat{K}$ to be determined. The boundary condition (10b) on $\hat{\psi}'$ states that $\delta v = 0$ at the two ends, and holds because the pressure is fixed there.

5. Explicit solution of the disturbance equations

Let $A(x)$ be arbitrary. Substitution shows $(9b,c)$, and the boundary conditions (10) in z to be satisfied if

$$a\hat{\psi} = A', \quad \hat{\phi} = A\bar{\Phi}_x, \quad \hat{T} = A\bar{T}_x \quad \text{and} \quad \hat{K} = -A\frac{\bar{G}'}{\bar{G}^2}. \tag{11}$$

$A(x)$ is determined by the remaining equation (9a). Thus

$$(\bar{G}A'')' - a^2\bar{G}A' + a^2\bar{G}'A = 0, \tag{12a}$$

$$A = 0 = A'' \text{ at } x = 0 \quad \text{and} \quad A'' = 0 \text{ at } x = X. \tag{12b,c,d}$$

Equation (12) determines the stability of the base flow to the three-dimensional disturbances (11). Primes in (12) denote differentiation in x. $X = \kappa L_c / Qd$, as defined in §2, and $\bar{G}$ is the pressure gradient in the base flow (5). The boundary conditions follow from those stated following (10). In particular, A vanishes at $x = 0$ because $\hat{T} = 0$ there.

The set (11) is not complete, but physical reasoning *suggests* that it includes the most unstable disturbances. In the base flow, fluid is cooled by thermal boundary layers that emerge from the discontinuity in wall temperature and grow to fill the channel downstream. Fluid on the centreline remains at the inlet temperature until the boundary layers growing from opposite walls merge. Inspection of the disturbance heat equation (9c) shows that $\hat{T}$ therefore vanishes outside the growing thermal boundary layers. The least-damped thermal disturbance therefore vanishes at the wall, has a single maximum within the boundary layer, and vanishes outside it. The thermal disturbance (11) has these properties.

The eigenvalue problem solved by Pearson *et al.* (1973, equation 29) is a special case of (12). Their (29) follows by substitution of their model pressure gradient (their (9)) in (12). The critical viscosity ratio obtained here therefore differs from that of Pearson *et al.* because their model does not accurately represent the base flow.

This formulation shows the stability of the plane flow to be determined by the pressure gradient $\bar{G}$. The theory makes concrete the intuitive analogy between flows with temperature-sensitive viscosity, and flows with solidification because the same eigenvalue problem (12) holds for both flows. Only the details of the pressure gradient change. The theory is illustrated in the rest of this work by applying it to variable-viscosity flow without solidification, i.e. with $c(T) = 1$. (Solidification could be incorporated in the computation of the base flow by a transformation due to Lee & Zerkle 1969.)
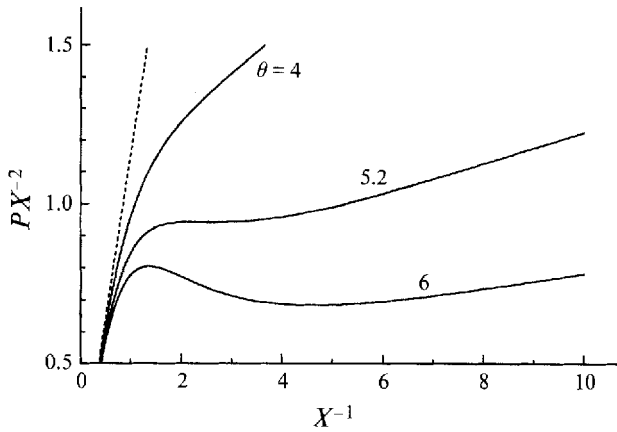
FIGURE 2. Relation between pressure drop and flow rate. Computed for viscosity $\mu = e^{-\theta T}$, and specific heat $c(T) = 1$. $PX^{-2} = d^4\Delta p/\mu_w\kappa L_c^2$, as defined in (15); $X = L_c/L_e = \kappa L_c/Qd$, as defined §2; and $\theta = \ln(\mu_w/\mu_i)$ is the logarithm of the ratio of wall to inlet viscosity, as defined in §6.

6. Base flow

Results for $\bar{p}(x)$ and $\bar{G}(x)$ are given here, as they determine the stability of the base flow. The calculations are for $c(T) = 1$, as noted above. The viscosity law is $\mu = e^{-\theta T}$, as used by Pearson *et al.* By the choice of units in §2, T vanishes at the wall, and is one at the inlet $x = 0$. θ is therefore the logarithm of the ratio of wall to inlet viscosity, i.e. $\theta = \ln(\mu_w/\mu_i)$.

Figure 2 shows the computed flow rate–pressure drop relation for $\theta = 4, 5.2$ and 6, the values of θ being chosen to illustrate the development of turning points in the relation. The pressure drop varies monotonically with Q if θ is less than a critical value of about 5.2. Above this critical value, the pressure–flow curve has two turning points, as in figure 2. The existence of the turning points follows from an argument used by Pearson *et al.* on their model problem. If the channel is either very short or very long, the pressure drop follows the Poiseuille law with the appropriate viscosity. Thus $\Delta p \propto \mu_i Q$ for a short channel ($Qd/\kappa L_c \equiv X^{-1} \to \infty$), and $\Delta p \propto \mu_w Q$ for a long channel. When plotted in the units introduced in §2, the pressure–flow curve thus has unit slope for $aQ/\kappa L_c \to 0$, and slope $\mu_i/\mu_w = e^{-\theta}$ for $aQ/\kappa L_c \to \infty$. For $\theta \gg 1$, the slope of the large-Q asymptote is small, and turning points in the pressure–flow curve are possible. These turning points are important for the stability of the plane flow.

Figure 3 shows the numerical solution for $\bar{G}$ for $\mu = e^{-\theta T}$, and $\theta = 4, 6$ and 8. This range of θ is chosen because the critical value of θ lies between 5 and 6 for a wide range of channel lengths: in this sense the figure shows a typical set of base states. Notice that $\bar{G}$ varies linearly with $x^{1/3}$ as $x \to 0$. This happens because the boundary layer initially grows as $x^{1/3}$, as shown in Appendix B, equation (B7). This weak singularity is allowed for in solving the stability problem (see §8).

Table 1 gives $\bar{G}(x)$ to five significant figures, to facilitate comparison of this and any subsequent work. These results were obtained on a grid of 12000×400.

7. Turning point instability

Equation (12) includes the turning-point instability suggested by figure 2, i.e. the base flow (5) is unstable to long waves $a \to 0^+$ whenever the pressure–flow curve has
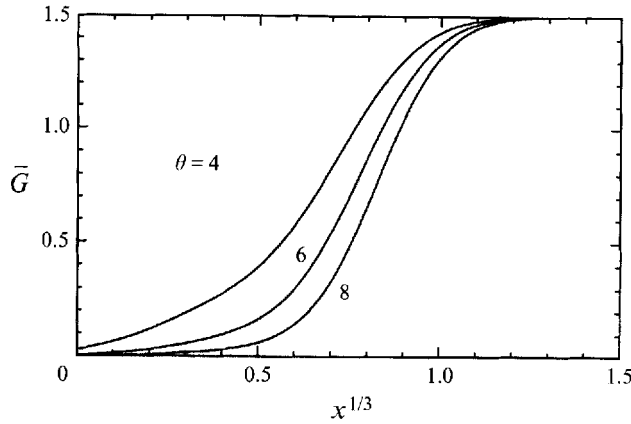
FIGURE 3. Computed pressure gradient ($\bar{G}$) as a function of $x^{1/3}$. X, viscosity law and specific heat as in figure 2. As defined §2, $\bar{G} = -d^3\bar{p}'_*(x)/\mu_w Q$, and $x = x_*/L_e$.

$x^{1/3}$	$\bar{G}$	$x^{1/3}$	$\bar{G}$
0.125	0.015700	0.875	1.1078
0.250	0.041187	1.000	1.3750
0.375	0.083240	1.125	1.4739
0.500	0.16110	1.250	1.4964
0.625	0.34430	1.375	1.4997
0.750	0.69490	1.500	1.5000

TABLE 1. Base flow for $\theta = 6$

turning points. First note that (12) is satisfied if $A' = 1$ and $a = 0$. This solution is trivial because the disturbance is independent of y, but suggests the non-trivial expansion

$$A(x) = x + a^2 A_1(x) + O(a^4). \tag{13}$$

Substitution in (12) shows that at order a^2

$$(\bar{G}A_1'')' - \bar{G} + x\bar{G}' = 0, \tag{14}$$

and A_1 satisfies the homogeneous boundary conditions $(12b,c,d)$. A_1 follows by quadrature. In particular, integration of (14) from $x = 0$ to $x = X$ followed by use of $(12c,d)$ shows the solution exists if $\int_0^X (\bar{G} - x\bar{G}')\,dx = 0$, i.e. if

$$\frac{d}{dX} \frac{P(X)}{X^2} = 0, \text{ where } P(X) = \int_0^X \bar{G}\,dx \tag{15}$$

is the dimensionless pressure drop.

Equation (15) determines $X(\theta)$, the channel length for which instability is possible for a given θ. The corresponding disturbance velocity and temperature are

$$\hat{u} = xU_x - U, \quad \hat{v} = 0, \quad \hat{w} = -xW_x, \quad \hat{T} = x\bar{T}_x, \tag{16}$$

by (8) and (11). The spanwise disturbance velocity $\hat{v}$ vanishes.

Equations (15) and (16) are readily interpreted. The (dimensional) pressure drop (Δp) is related to $\bar{G}$ by $\Delta p = (\mu_w Q^2/\kappa d^2) \int_0^X \bar{G}\,dx$ where $X = \kappa L_c/Qd$, as defined in
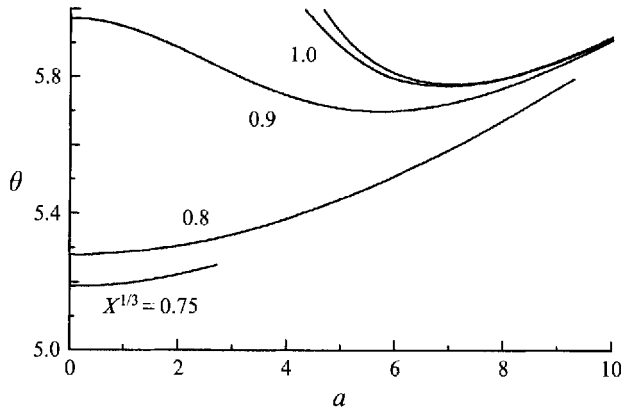
FIGURE 4. Neutral stability curve with $X^{1/3}$ as a parameter. The top, unlabelled curve is for $X \to \infty$. θ, X, viscosity law and specific heat as in figure 2. As defined in §4, $a = a_* L_e$, where a_* is the dimensional wavenumber.

§2. $\bar{G}$ is independent of Q, since Q does not appear in the dimensionless boundary value problem (5) defining the plane flow, as noted in the penultimate paragraph of §3. Thus

$$\frac{d}{dQ}\Delta p = -\frac{\mu_w L_c}{d^3}X^2\frac{d}{dX}\frac{P(X)}{X^2}.$$

Equation (15) is thus the condition for the pressure drop–flow rate curve to have a turning point. Similarly

$$\hat{u} = -d\frac{\partial \bar{U}_*}{\partial Q} \quad \text{and} \quad \hat{T} = -\frac{Q}{\Delta T}\frac{\partial \bar{T}_*}{\partial Q}.$$

All quantities on the right-hand side of this equation are dimensional. The differentiation in Q is performed at fixed (dimensional) x_*.

These results are discussed in more detail at the end of §8.

8. Solution of (12) for arbitrary a

Equation (12) is singular at $x = 0$ because $\bar{G}'(x)$ is singular there, as noted in the discussion of figure 3. The singularity was removed by the substitution $x = s^3$, and the transformed equations were integrated from $s = 0$ to $s = S \equiv X^{1/3}$ by a second-order Runge–Kutta scheme with uniform steps in s. Appendix B gives details.

Figure 4 shows the computed neutral stability curve with channel length $X = S^3$ as a parameter. If S exceeds a critical value (S_T), the neutral curve has two turning points: a local maximum at $a = 0^+$, and a local minimum for $a = a_c$. For $S \leqslant S_T$, these turning points coalesce to form an absolute minimum at $a = 0^+$. The turning-point instability (15) occurs when the turning-point at $a = 0^+$ is an absolute minimum. It is shown below that this happens for $S < S_T \approx 0.84$. Since $\theta_c \approx 6$ for this value of S_T, the pressure gradient is given roughly by the middle curve in figure 3. That figure shows that $\bar{G}$ increases most strongly with distance for $x^{1/3} < 0.8$. This suggests that the turning-point instability is favoured when $\bar{G}$ increases strongly with x. This is consistent with the analysis in Appendix C of another example of the instability. There, the dimensional viscosity law is $\mu = \mu_0 e^{-\gamma T}$, and the wall temperature is taken to decrease linearly with x. The viscosity increases exponentially with x, and so too
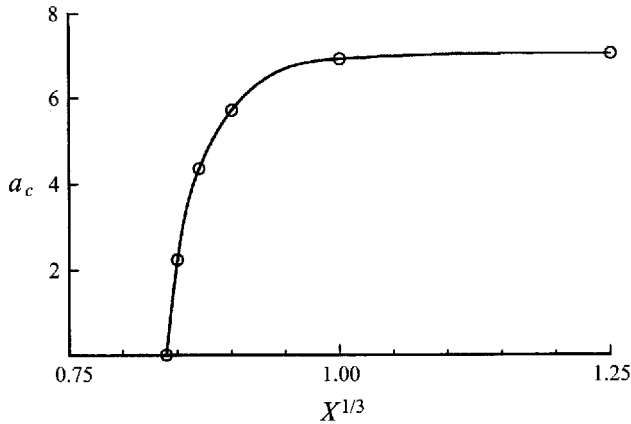
FIGURE 5. Variation of critical wavenumber (a_c) with $X^{1/3}$. X, viscosity law and specific heat as in figure 2; dimensionless wavenumber as in figure 4.
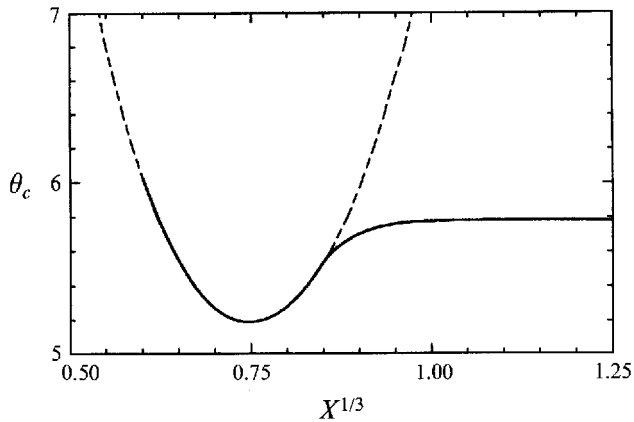

FIGURE 6. Variation of critical viscosity parameter (θ_c) with $X^{1/3}$.
θ, X, viscosity law and specific heat as in figure 2

does $\bar{G}$. The heuristic reasoning above suggests that a turning-point instability should occur owing to the rapidly increasing pressure gradient. The calculations in Appendix C support this expectation.

Figure 5 shows the variation of a_c with $S = X^{1/3}$, where X is the dimensionless channel length, as defined in §2. a_c was found as follows. Near the critical point on the neutral stability curve for a given S, a is a doubly valued function of θ. As the critical θ is approached, the mean of the values of a approaches a_c. The most unstable wave has non-zero wavelength if $S \geqslant S_T$, where the figure shows that $0.84 < S_T < 0.85$, i.e. $X \approx 0.6$. For long channels ($S \to \infty$) $a_c \to 7.03$. The corresponding dimensional wavelength is $0.894Qd/\kappa$. The striking feature of figure 5 is that the most unstable wavelength is at least comparable with the entry length for all X. The geological implications of this are discussed below, in §9.

Figure 6 shows the variation of θ_c with $S = X^{1/3}$. The minimum $\theta_c = 5.19$ at $S = 0.75$. In an infinite channel $\theta_c = 5.78$, corresponding to a viscosity ratio of 324. This plot resembles a plot of similar results for the model of Pearson *et al.*, but
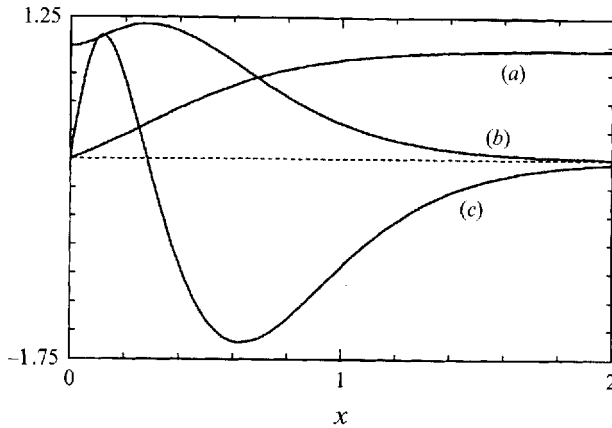
FIGURE 7. Eigenfunction of (12) for an infinite channel ($X \to \infty$) and $\theta = 5.78$ (approximately the critical value). (a) $A(x)$; (b) $A'(x)$; and (c) $A''(x)$. Viscosity and specific heat as in figure 2.

is quantitatively different. For example, their critical viscosity ratio for an infinite channel is about one-tenth that given here.

Figure 7 shows the eigenfunction for an infinite channel. The thermal disturbance $\hat{T} = AT_x$. This vanishes downstream because A becomes constant, as in curve (a), and $\bar{T}_x$ vanishes. The figure also shows why absolute instability is possible in this flow. Because $A' = a\hat{\psi}$, curve (b) shows that $\hat{\psi} \neq 0$ even at $x = 0$. The source term for the instability is the second term on the right-hand side of (9c), particularly $-\hat{u}\bar{T}_x$. This is non-zero even at the inlet because $\hat{u} \sim \hat{\psi}$, by (8a). Temporal growth is therefore possible at a fixed point if the viscosity ratio is large enough for the source mechanism to overcome the stabilizing effect of heat losses to the walls.

9. Discussion

The set (11) of disturbances is not complete, but physical reasoning suggests that it contains the most unstable disturbances. In any case, this study can be used to test any subsequent exhaustive analysis of the instability. This solution of the disturbance equations is the small-amplitude limit of the steady, finite-amplitude solution (6). In fact, substitution shows that if $\epsilon \ll 1$ is a given small parameter, the expressions

$$\xi = x + \epsilon A(x)\cos ay + O(\epsilon^2) \text{ and } \psi = y - \epsilon\frac{A'(x)}{a}\sin ay + O(\epsilon^2) \qquad (17)$$

satisfy (7) to order ϵ if $A(x)$ satisfies (12b). (To avoid confusion, note that (17) and (12b) together imply that $\xi(0, y) = 0$, as required by its definition in §3.) The neutral disturbances studied in §§5–8 are thus of the form (6).

This analysis predicts the most unstable wavelength to be either greater than, or comparable with, the thermal entry length for all channel lengths. The parameters for dyke flows, estimated by Delaney & Pollard (1982) and cited earlier in §2, correspond to thermal entry lengths of 500–1000 km. Features of this scale on the Earth are tectonic rather than geological: they are not observable on an outcrop. But the fingers reported by Pollard et al. (1975) have diameters of a few metres, with comparable wavelengths. The simplest explanation is that fingering occurs only when magmatic systems are about to solidify so that flow rates have fallen sufficiently to make the wavelength of geological scale. This is compatible with observations of an Hawaiian

eruption by Richter *et al.* (1970), where isolated vents formed only after the initial eruption had subsided. A second explanation is suggested by work of Whitehead & Helfrich (1991). That study coupled the dyke flow to an elastic magma chamber, and analysed the channel flow by an approach similar to that of Pearson *et al.* Whitehead & Helfrich (p. 4155) interpret their results to imply that the preferred wavelength is *short* compared with the channel length. If this interpretation were true, chamber elasticity would presumably be a central part of geological fingering. But the authors' interpretation of their analysis seems incorrect. Scrutiny of their growth rate–wavenumber plot (Whitehead & Helfrich, figure 10) shows both growth rate and wavenumber to be normalized by a factor (namely 'df/dw') vanishing at the neutral point. Their analysis thus implies that the most unstable waves are *long* compared with the channel length, rather than short.

The implications of the finite-amplitude instability can be understood by scaling. Suppose the dimensional viscosity $\mu = \mu_0 e^{-\gamma T}$. In the finite-amplitude instability, the large viscosity variation will confine the flow to tubes of radius R, in which the temperature difference is the rheological scale γ^{-1}. The cooling rate is determined by balancing convection against conduction across the tube, i.e. $w T_x \sim \kappa \gamma^{-1}/R^2$. But $w R^2 \sim Q_3$, the volume flow in the tube. The entry length (L_3) in the three-dimensional flow is thus $\Delta T / T_x \sim \theta Q_3/\kappa$, where $\theta = \gamma \Delta T$. If a single wavelength of the instability produces one finger, $Q_3 \sim Q\lambda \sim Q L_e$, where Q and L_e are the volume flow and entry length in the unstable plane flow. The ratio of entry lengths is thus $L_3/L_e \sim \theta Pe$. The instability reduces the heat loss, and increases the entry length by concentrating the volume flow, and also by reducing the temperature difference available to drive heat flow from ΔT to γ^{-1}. This qualitative argument is supported by a simple solution for steady, finite-amplitude flow, describing the streamwise evolution of tubular fingers. That solution is, however, beyond the scope of this work.

Appendix A. Stream functions for Hele-Shaw flow

Let ϕ and ψ be independent, but otherwise arbitrary, functions of x, y and z. Any three-dimensional solenoidal vector field V can be written in Euler's form

$$V = \text{grad}\psi \times \text{grad}\phi \tag{A 1}$$

(Ericksen 1960, §32). ϕ and ψ are constant on streamlines because $V \cdot \text{grad}\phi = 0 = V \cdot \text{grad}\psi$. Each streamline is thus specified as the intersection of surfaces of constant ϕ and ψ.

Equation (A1) simplifies for Hele-Shaw flow. Because p is then independent of z, all streamlines passing through the line $x = \text{const}$, $y = \text{const}$ have a common projection on the $(x, 0, y)$-plane. One of the two families of surfaces needed to locate the streamline can therefore be taken as independent of z. We take $\psi = \psi(x, y)$ to get (2).

ϕ can be taken as constant on the walls, because the kinematic condition ($w = 0$) requires $\nabla\phi \times \nabla\psi = 0$. But ϕ and ψ are independent families of surfaces, and $\nabla\psi \neq 0$. Thus $\nabla\phi = 0$ on the walls. We choose $\phi(x, y, \pm 1) = \pm 1/2$.

Appendix B. Numerical method

B.1. *Plane flow*

Equation (5) is transformed, without approximation, to remove the singularity at $x = 0$ and $|z| = 1$. Let $s = x^{1/3}$, and let δ be an arbitrary function of s. Also let $n = (1 - z)/\delta$, and let

$$\phi = \tfrac{1}{2} - \tfrac{3}{2}\delta^2 f(s, n) \quad \text{and} \quad T = h(s, n). \tag{B 1a, b}$$

Without approximation, (5) becomes

$$(\delta/s)^2 \left[\tfrac{1}{2}\delta(f_n h_s - f_s h_n) - \delta_s f h_n \right] = h_{nn} \quad \text{and} \quad \tfrac{2}{3}\bar{G}(1 - n\delta) = \mu f_{nn}. \tag{B 2a, b}$$

$$\text{On} \quad n = 0, \ f = f_n = 0 = h; \quad \text{on} \quad n = \delta^{-1}, \ h_n = 0. \tag{B 2c, d}$$

As noted above (2), this work correctly includes all convective terms in the heat balance. Specifically, in the transformed heat equation (B2a), the first term on the left accounts for convection in the s-direction; the second and third terms account for convection perpendicular to the parabolic coordinate surfaces $n =$const. The transformed equation thus states the balance between heat convection and diffusion perpendicular to the walls.

The remaining boundary condition determines $\bar{G}$. It is $\phi = \tfrac{1}{2}$ on $z = 1$, which can be written $\tfrac{1}{2} = \int_0^1 U \, \mathrm{d}z$. Integration by parts, followed by elimination of U_z using (5b), shows that

$$\tfrac{1}{2} = \bar{G} \int_0^1 \frac{z^2}{\mu(T)} \, \mathrm{d}z. \tag{B 3}$$

The use of this relation is explained below. (See (B6).) The initial condition is that $h = 1$ at $x = 0$.

δ is chosen as

$$\delta = \begin{cases} s & \text{if } s \leqslant s_1, \\ s_1 & \text{if } s > s_1. \end{cases} \tag{B 4a, b}$$

Equation (B4) removes the singularity at $x = 0$ from the solution. As $s \to 0$, $T \to 1$ for all z, and (B3) shows that $\bar{G} \to \bar{G}(0)$, $= \tfrac{3}{2}\mathrm{e}^{-\theta}$ for the viscosity law $\mu = \mathrm{e}^{-\theta T}$. The coefficients in (B2) are thus asymptotically independent of s as $s \to 0$ because $\delta \to s$. As $s \to 0$, the solution of (B2) thus approaches the similarity solution defined by (B1) with f and h satisfying

$$fh' + h'' = 0 \quad \text{and} \quad \tfrac{2}{3}\bar{G}(0) = \mu f'', \tag{B 5a, b}$$

$$f(0) = f'(0) = 0 = h; \ h(\infty) = 1. \tag{B 5c, d}$$

This similarity solution extends the Lévêque solution for isoviscous flow to variable-viscosity flow. (For the isoviscous solution see e.g. Worsøe-Schmidt 1967.)

The domain is $0 \leqslant s < \infty$, $0 \leqslant n \leqslant \delta^{-1}$. For computation of h (but not $\bar{G}$, as discussed below), this curvilinear domain can be replaced by the rectangular domain $0 \leqslant s < \infty$, $0 \leqslant n \leqslant n_1$, where $n_1 = 1/s_1$ is constant. This is done, to arbitrary precision, by choosing n_1 to be large enough that $h \to 1$ between the curves $n = \delta^{-1}$ and $n = n_1$. The appropriate choice depends on the viscosity parameter θ. For $5 < \theta < 15$, $8 < n_1 < 16$. n_1 increases with θ because the boundary-layer thickness is larger than $x^{1/3}$ for $\theta \gg 1$.

The whole curvilinear domain must be used to compute $\bar{G}$ from T. Integral (B3) is thus split in two. The first term gives the contribution from the area between the curves $n = \delta^{-1}$ and $n = n_1$. This term is evaluated explicitly because $h = 1$ in this

subdomain. The remainder is evaluated numerically, at each step. $\bar{G}$ is thus found from

$$\tfrac{3}{2} = \bar{G}\left[\frac{(1 - n_1\delta)^3}{\mu(T_c)} + 3\delta \int_0^{n_1} \frac{(1 - n\delta)^2}{\mu(T)}\,\mathrm{d}n\right]. \tag{B6}$$

Here $n_1 = 1/s_1$, as used above. T_c is the centreline temperature at x.

The asymptotic expansion of $\bar{G}(x)$ for $x \to 0$ is found from (B6) by expanding in powers of $\delta = x^{1/3}$. For the viscosity law $\mu = \mathrm{e}^{-\theta T}$, the first two terms are

$$\bar{G}\mathrm{e}^\theta = \tfrac{3}{2} + G_1 x^{1/3}, \quad \text{where} \quad G_1 = \tfrac{9}{2}\lim_{n\to\infty}(n - f'). \tag{B7}$$

The first term on the right gives the Poiseuille law. The second term is the correction to the Poiseuille law due to the displacement effect of the cold boundary layer. G_1 is found by solving (B5). Equation (B7) is used to verify the numerical method, and to develop the series (B8) used to start the solution of the stability problem.

Equation (B2a) is converted to difference form using backward differences in s and centred differences in n. Given h and $\bar{G}$ at s, (B2b) is solved by a second-order Runge–Kutta method. This gives $f(s)$ and $f_n(s)$ simultaneously. Equation (B2a) is then used to predict $h(s + \mathrm{d}s)$, and $\bar{G}(s + \mathrm{d}s)$ is found from (B6) by the trapezoidal rule. Picard iteration is then used to find final values for f, h and $\bar{G}$ at $s + \mathrm{d}s$.

The scheme was tested against the (isoviscous) Graetz–Nusselt solution (e.g. Brown 1960), and against asymptotic analysis for $\mu = \mu_0\mathrm{e}^{-\theta T}$ and $\theta \to \infty$ (Ockendon & Ockendon 1977). The method was also tested against a slower numerical method. In that method, the grid is uniform in x and z, and the singularity at $x = 0$ is treated by setting $w = 0$ for the first 50 steps in x.

Convergence of the scheme was tested as usual, by plotting variables of interest, such as the eigenvalue a of (12), against $\mathrm{d}s$ and $\mathrm{d}n$.

B.2. *Eigenvalue problem (12)*

As noted in the text, (12) is singular at $x = 0$. The singularity was removed by the substitution $x = s^3$, and the transformed equation was integrated from $s = 0$ to $S = X^{1/3}$ by a second-order Runge–Kutta method with uniform steps in s. The solution was started at a small positive value of $s = s_0$ using the series

$$A = x + \tfrac{1}{6}a^2 x^3 - \tfrac{3}{70}a^2 G_1 x^{10/3} + O(x^{11/3}). \tag{B8}$$

G_1 is the coefficient of $x^{1/3}$ in the series expansion of $\bar{G}$ about $x = 0$, as defined by (B7) above. Equation (B8) is derived by writing (12a) as $(\bar{G}(A'' - a^2 A))' = -2a^2\bar{G}'A$. The right-hand side is $O(x^{1/3})$, and integration in x allows (17) to be developed.

Results were obtained using $\mathrm{d}s = 0.001$–0.00025. The *eigenvalue a* is independent of s_0 to the precision stated if $s_0 < 0.025$. The *eigenfunction* depends on s_0 unless $0.00125 < s_0 < 0.025$. At the upper end of this range, more terms are needed in the starting series (B8); at the lower end, use of (B8) is limited by machine precision.

The limiting case $S \to \infty$ was calculated by cutting the line $0 < s < \infty$ in two. From figure 3 (and table 1), $\bar{G}'$ can be taken as zero for $s \geqslant s_2 = 1.5$. Equation (12) can be thus be solved explicitly in the interval $s_2 < s < \infty$, and is equivalent to

$$\mathscr{L}A \equiv A'' + aA' = 0. \tag{B9}$$

Because A'' and A' must be continuous at S, (B9) thus gives the boundary condition at S for the numerical solution of (12) on the interval $0 < s < S$. When the channel is infinite, this shooting method suffers from induced instability (Fox & Mayers 1968, p. 225). The method then accurately determines the eigenvalue and critical viscosity

ratio, but gives the eigenfunction much less accurately. (In this case, the eigenfunction was determined to within a fraction of a percent.)

Appendix C. Parallel flow for $T_w = T_i - \beta x$ and its stability

$\beta > 0$ and T_i are dimensional constants. This flow is notable because the analysis is simplified. The base flow is unidirectional, and the disturbance equations are separable. $\bar{G}$ proves to increase exponentially with x, and there is a turning-point instability. The results are used in the text (§8) to argue that a turning-point instability is favoured when $\bar{G}$ increases strongly with x.

Fluid enters the channel at $x = 0$ at temperature T_i, and T_w falls linearly with x for all $x > 0$. In the streamwise distance ($L_e = dPe$) taken for heat to diffuse across the channel, T_w falls by $\Delta T = \beta L_e$. The parallel flow can be expected to occur for $x \gg L_e$, and the temperature difference between the centreline and wall is therefore proportional to ΔT. Dimensionless variables are therefore defined as in §2, *except* that the reference temperature is T_i, the reference temperature difference ΔT, and the pressure unit $\mu_i Q L_e / d^3$. As in the text, dimensional variables are starred. The viscosity law is $\mu_* = \mu_i e^{-\gamma(T - T_i)}$ where μ_i and γ are constants.

C.1. *Base flow*

Let $\bar{T}(z) = -x + H(z)$, $U = U(z)$, $W = 0$ and $\bar{G} = e^{\theta x}g$, where g is dimensionless, and proves to be constant, as noted in the comment following (C2). Because $\mu_w = \mu_i e^{\theta x}$, the equation for $\bar{G}$ implies $-\bar{p}_x \equiv \bar{G}_* \propto \mu_w Q / d^3$. The pressure gradient thus increases exponentially with x in this flow, because the viscosity does. The dimensionless constant g accounts for the details of the velocity profile. By definition of g

$$\theta g = \frac{\gamma \beta d^4 \bar{G}_*}{\kappa \mu_w} \quad \text{and} \quad \theta \equiv \gamma \Delta T = \frac{\gamma \beta Q d}{\kappa}. \qquad (C\,1a,b)$$

θg is the pressure gradient measured in units independent of Q. θ is a measure of flow rate, and controls the ratio of wall to centreline viscosity.

By substitution in (5), H and $U(z)$ satisfy

$$0 = g z e^{\theta H} + U', \quad 0 = U + H'', \qquad (C\,2a,b)$$

$$H'(1) + \tfrac{1}{2} = H(1) = U(1) = 0 = H'(0). \qquad (C\,2c,d,e,f)$$

Equation (C2c) follows from (C2b) and the volume constraint $\int_0^1 U \, \mathrm{d}z = \tfrac{1}{2}$. (C2) is solved by marching from $z = 1$ to $z = 0$, and using Newton's method to choose g to satisfy (C2c). By (C2), g is independent of x, and depends only on θ.

Figure 8 shows the relation between pressure gradient (θg), defined by (C1a) and flow rate (θ), defined by (C1b). Notice that $\theta H(0) = \ln(\mu_w/\mu_c)$, where μ_c is the viscosity on the centreline. The figure shows that θg has a maximum of 3.855 at $\theta H(0) = 1.982$, corresponding to a viscosity ratio $\mu_w/\mu_c = 7.257$. This maximum is associated with a turning-point instability, as shown below. It exists because $\theta g \to 0$ both at $\theta = 0$ and at ∞. θg vanishes at the origin because the Poiseuille law for isoviscous flow requires $\bar{G}_* \propto \mu_w Q / d^3$. θg thus vanishes for $\theta \to 0$, by (C1a). θg also vanishes as $\theta \to \infty$, because the large viscosity ratio then confines the flow to a thin layer centred on $z = 0$. The dimensional pressure gradient ($\bar{G}_*$) is thus proportional to the centreline viscosity, rather than μ_w, and is therefore exponentially small in Q, i.e. in θ. More precisely, an elementary asymptotic analysis shows that for $\theta \to \infty$, $\theta g \sim (\theta/2c_0)^4 \exp(-\theta H(0))$, where $\theta H(0) \sim \tfrac{1}{2}\theta + c_1$, $c_0 = 1.688$ and $c_1 = -1.710$. The
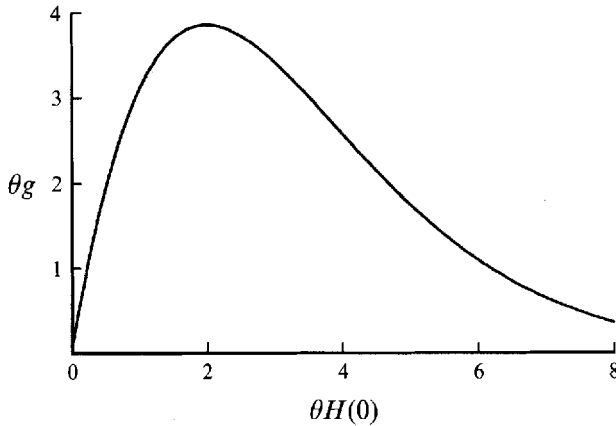
FIGURE 8. Pressure gradient–flow rate relation for the parallel flow.
θg and $\theta H(0)$ are defined by (C1).

pressure gradient is thus more sensitive to flow rate in the parallel flow than in the entry flow, because the dimensional centreline temperature varies with flow rate here.

C.2. *Stability*

It is convenient to use (8a) to express the disturbance equations (9) in terms of $\hat{u}$ rather than $\hat{\phi}$. Let $\hat{k} = e^{\theta x}\hat{K}$. Then for the parallel base flow, (9) becomes

$$\hat{\psi}'' + \theta\hat{\psi}' - a^2\hat{\psi} = ag\hat{k}, \quad \hat{u}_z + (a\hat{\psi} + g\hat{k} - \theta\hat{T})U'(z) = 0, \quad U\hat{T}_x = \hat{T}_{zz} + \hat{u}. \quad \text{(C 3)}$$

a is the disturbance wavenumber in the spanwise (y) direction, as defined in §4.

The coefficients in (C3) depend only on z, so that Fourier transformation in x is possible. In particular, (C3) admits a solution in which $\hat{\psi}, \hat{u}$ and $\hat{T}$ are independent of x. For these disturbances, (C3a) requires $a\hat{\psi} + g\hat{k} = 0$ *provided $a \neq 0$* so that the disturbance varies in the spanwise coordinate y. Equations (C3b) and (C3c) thus simplify to

$$\hat{T}_{zz} = \hat{u}, \quad \hat{u}_z = \theta\hat{T}U'(z), \quad \text{(C 4a,b)}$$

$$\hat{T}(1) = \hat{u}(1) = 0 = \hat{T}'(0). \quad \text{(C 4c,d,e)}$$

Equation (C4b) shows that the disturbance to the (total) shear stress vanishes for these disturbances, i.e., $\delta(\mu u_z) = 0$, so that the perturbation pressure vanishes. This happens because both disturbance and base flow are unidirectional. p therefore depends only on x in this Hele-Shaw flow, as use of (1a,b) shows. In other words, the perturbation pressure gradient vanishes for $a \neq 0$, as in (C5b).

Notice that a does not appear in the eigenvalue problem (C4), and is therefore arbitrary. In this Hele-Shaw analysis of the parallel flow there is thus no wavenumber selection.

By substitution, (C4) admits the solution

$$\hat{T} = (\theta H)_\theta, \quad \hat{u} = (\theta U)_\theta \quad \text{(C 5a,b)}$$

provided $(\theta g)_\theta = 0$. The unidirectional base flow (C1) therefore loses stability to unidirectional disturbances at the turning-point in the θg–θ curve shown in figure 8. Thus $\theta_c = 5.838$, $(\theta H_0)_c = 1.982$. The ratio of wall to centreline viscosity is then

$\exp(\theta H_0) = 7.257$ (Morris 1988). In the entry flow, the maximum viscosity ratio in the neutrally stable flow occurs before fluid on the centreline begins to cool, and is about 324 in a channel of infinite length. The parallel flow is less stable than the entry flow because the pressure gradient is more sensitive to Q in the parallel flow.

These remarks also hold for disturbances with non–zero wavenumber, b, in the primary (x) direction provided $a \gg b$.

REFERENCES

BLOTTNER, F. G. 1975 Computational techniques for boundary layers. *NATO–AGARD Lect. Ser.* no. 73, pp. 3.1–3.51.

BROWN, G. M. 1960 Heat transfer in laminar flow in a circular or flat conduit. *AIChE J.* **6**, 179–183.

DELANEY, P. T. & POLLARD, D. D. 1982 Solidification of basaltic magma during flow in a dyke. *Am. J. Sci.* **282**, 856–885.

DUPRET, F. & DHEUR, L. 1992 Modelling and numerical simulation of heat transfer during the filling stage of injection moulding. In *Heat and Mass Transfer in Materials Processing* (ed. I. Tanasawa & N. Lior). Hemisphere.

ERICKSEN, J. L. 1960 Tensor fields. In *Handbuch der Physik*, III/I. Springer.

FOX, L. & MAYERS, D. F. 1968 *Computing Methods for Scientists and Engineers*. Oxford.

LANDAU, L. D. & LIFSHITZ, E. M. 1987 *Fluid Mechanics*. Pergamon.

LEE, D. G. & ZERKLE, R. D. 1969 The effect of solidification on laminar–flow heat transfer and pressure drop. *J. Heat Transfer* **91**, 583–585.

MORRIS, S. 1988 An instability caused by spanwise viscosity variations in channel flow. *Bull. Am. Phys. Soc.* **33**, 2247.

MURASE, T. & MCBIRNEY, A. R. 1973 Properties of some common igneous rocks and their melts at high temperatures. *Geol. Soc. Am. Bull.* **84**, 3536–3592.

OCKENDON, H. & OCKENDON, J. R. 1977 Variable–viscosity flows in heated and cooled channels. *J. Fluid Mech.* **93**, 737–746.

PEARSON, J. R. A. 1976 Instability in non–Newtonian flow. *Ann. Rev. Fluid Mech.* **8**, 163–181.

PEARSON, J. R. A. 1985 *Mechanics of Polymer Processing*. Elsevier.

PEARSON, J. R. A., SHAH, Y. T. & VIEIRA, E. S. A. 1973 Stability of non–isothermal flow in channels–I. Temperature–dependent Newtonian fluid without heat generation. *Chem. Engng Sci.* **28**, 2079–2088.

POLLARD, D. D., MULLER, O. H. & DOCKSTADER, D. R. 1975 Form and growth of fingered sheet intrusions. *Geol. Soc. Am. Bull.* **86**, 351–363.

RICHTER, D. H., EATON, J. P. MURATA, K. J. AULT, W. U. & KRIVOY, H. L. 1970 Chronological narrative of the 1959–1960 eruption of Kilauea volcano, Hawaii. *US Geol. Survey Prof. Paper* 537–E.

TAN, C. T. & HOMSY, G. M. 1986 Stability of miscible displacements in porous media. *Phys Fluids* **29**, 3549–3556.

TAN, C. T. & HOMSY, G. M. 1988 Simulation of nonlinear viscous fingering in miscible displacement. *Phys. Fluids* **31**, 1330–1338.

WHITEHEAD, J. A. & HELFRICH, K. R. 1991 Instability of flow with temperature– dependent viscosity: a model of magma dynamics. *J. Geophys. Res.* **96**, 4145–4155.

WORSØE–SCHMIDT, P.-M. 1967 Heat transfer in the thermal entrance region of circular tubes and annular passages with fully developed laminar flow. *Intl J. Heat Mass Transfer* **10**, 541–551.